J Mater Sci (2011) 46:7206–7213
DOI 10.1007/s10853-011-5676-4

Investigation of the electrical and mechanical properties of short sisal fiber-reinforced epoxy composite in correlation with structural parameters of the reinforced fiber

Annapurna Patra · Dillip Kumar Bisoyi

Received: 21 March 2011 / Accepted: 30 May 2011 / Published online: 10 June 2011

Abstract Chemical modification of the sisal fiber is done through dewaxing. Increment in the degree of crystallinity, crystallite size, and bulk density are observed in case of the dewaxed sisal fiber. The partial removal of wax, hemicellulose, and lignin content is confirmed from the FTIR spectra. Better flexural strength and tensile strength are observed in case of dewaxed sisal fiber-reinforced epoxy composite (DSFREC) in comparison to the raw sisal fiber-reinforced epoxy composite (RSFREC). This may be due to the improvement in the adhesion between the fiber and matrix. Lower values of dielectric constant (ε_r) and dielectric loss ($\tan\delta$) are also observed in case of DSFREC. The shifting of M''_{max} toward higher frequency side with rise in temperature ascribing a correlation between motions of mobile ions and suggests a spread of relaxation times. Moreover, the structural parameters of the fiber are correlated with the mechanical and electrical properties of the composite.

Introduction

The study of natural fiber-reinforced polymer composite (NFRPC) materials is a fast growing area of research. This rapidly expanding field is generating many exciting new high-performance materials with novel properties. Easy processing, environment friendly nature, low cost, excellent insulation properties, and light weight have made NFRPC a smart material with versatile applications like in automobiles, aerospace, injection molded products, coatings, adhesives, fire-retardants, packaging materials, consumer goods etc. [1, 2]. Insulation resistance and dielectric strength of lignocellulosic fibers give an indication of their current leakages at certain voltages, moisture content and stability under electric fields [3]. Now a days composite as a dielectric is becoming more popular and studies of electrical properties of NFRPC are therefore very important. The study of electrical properties of such materials enable us to know the various electrical applications of these materials such as in suspension insulators, switch boards, antistatic applications etc. [4, 5]. Among all the natural fibers, sisal fiber in chopped, continuous, and woven forms has been found to be most suitable for application in polymer composites because of its superior properties like high cellulose content, high tensile strength, and yet cheaper in price [6].

Sisal like any other lingo-cellulosic fibers acts as a reinforcing material in the polymer composites. Surface of sisal fiber can be modified chemically and physically with an aim to reduce moisture sensitivity so as to increase the adhesion between fiber and matrix [7, 8]. Chemical treatment of natural fiber often causes defibrillization, which also contributes to the increased reinforcing efficiency of the fibers in the composite [9]. The removal of surface impurities which is a part of purification is advantageous for fiber–matrix adhesion as it facilitates both mechanical interlocking and the bonding reaction at the interface. In this regard, dewaxing is a very suitable conventional technique [10].

This article investigates the effect of dewaxing on the structural, vibrational properties of sisal fiber including electrical and mechanical properties of short sisal fiber-reinforced epoxy composite. An attempt has also been made to correlate the structural, vibrational properties of the fiber to the mechanical and electrical properties of the polymeric composite system.

A. Patra (✉) · D. K. Bisoyi
Department of Physics, National Institute of Technology Rourkela, Rourkela 769008, India
e-mail: annapurna.patra@gmail.com

Experimental

Materials and methods

The sisal fiber is obtained from the Sisal Research Station, Indian Council of Agricultural Research, Bamara, Orissa, India having a diameter of 170–300 μm.

Unmodified liquid epoxy resin based on Bisphenol A, of grade LY 556 along with hardener HY 951 is provided by B. Mukesh & Co., Kolkata, India. The density of the resin is 1.15 g/cc, whereas the hardener density is 0.97 g/cc.

Treatment of fiber

Fibers as received are washed with distilled water to remove the surface dirt present in the fibers and then the fibers are dried in an air circulating oven at a temperature of 100 °C until it gains a constant weight. Then the fibers are designated as raw sisal fibers.

For dewaxing the fibers are cooked in a mixture of (1:2) ethanol and benzene, as done earlier by Roy [11], for 12 h so that it attains a *hohlraum* character which means the substances lying in layers with free spaces in between [12]. During this process the fibers are cooked in the solution under gradual rise and fall of the temperature of the bath from 30 to 55.5 °C. This process of heating and cooling was done intermittently per every 2 h for a period of 12 h. Finally, the fiber bundles are removed from the mixture at a temperature of 30 °C. In order to remove excess mixture, the fibers are washed with distilled water. After washing, the fibers are again dried in an air circulating oven at a temperature of 100 °C until it gains constant weight. Then the fibers are designated as dewaxed sisal fibers.

Fabrication of composite plate

A handmade wooden mold is designed for the fabrication of the randomly oriented raw sisal fiber-reinforced epoxy composite (RSFREC) and dewaxed sisal fiber-reinforced epoxy composite (DSFREC). First, a releasing plastic is spread over the bottom of the wooden mold. Heavy duty silicon spray is applied to the plastic sheet for easy removal of the composite plate. The fibers are cut into 20 mm length and distributed uniformly at the bottom of the mold which is prepared before. Fifteen volume percentage of the fiber is used for the fabrication of the composite. Initially, epoxy and hardener are mixed together on a weight percentage of 10:1 to form a matrix. The matrix is poured over the fibers evenly then pressed and pushed down with the iron roller to avoid and eliminate the air bubbles. Finally, load is given to it to remove excess matrix and left for curing at room temperature for 24 h.

Characterization

In order to identify the effect of treatment on the micromolecular structures of sisal fiber, wide angle X-ray diffraction (WAXD) spectra are collected by PHILIPS PAN analytical PW1830 with Cu-K_α radiation from 10° to 45° with a scan speed of 0.04°/s. The crystallite sizes of the fibers are determined by modified Scherer's formula whereas the degree of crystallinity is computed by comparing the areas under crystalline peak and amorphous curve i.e., the area under the crystalline peak around 22.5° is compared with sum of the areas of amorphous peaks around 15° and 34° by peak fit software [13, 14]. Chemical compositions of the raw and dewaxed sisal fibers are investigated by the Perklin Elmer FTIR spectrometer spectrum RX-1 in the mid IR range i.e., from 400 to 4000 cm^{-1}. The density measurements of the fiber are done as per ASTM D3800-99. The bundle of fibers are weighed and denoted as W_a. Then this bundle of fiber is immersed in benzene having a density (ρ_b) 0.875 g/cc. The immersed fiber's weight is denoted as W_i. The bulk density (ρ) of the fiber was calculated by the following equation:

$$\rho = \rho_b W_a/(W_a - W_i).$$

The fractured surfaces of sisal fibers and composites are examined by SEM (JEOL JSM-6480 LV). In order to evaluate the flexural strength and tensile strength of the composites three point bending test and tensile test are carried out by INSTRON1195, respectively. The randomly oriented RSFEPC and DSFREC specimens are cut as per the ASTM D790 and ASTM D3039 to measure the flexural strength and tensile strength, respectively. The sample size for flexural measurement is 13 × 30 × 5 mm with a crosshead speed of 2 mm/min with a gauge length of 50 mm whereas for tensile measurement the sample size is 200 × 30 × 5 mm with crosshead speed of 1 mm/min with gauge length of 120 mm [15]. The reported data is the average of the five successful tests.

For electrical measurements, disk shaped samples having ~15 mm diameter are cut out of the composites and are polished to make a thickness of 2 mm. The circular surfaces of the test samples are polished and coated with conductive silver paste. The electrical measurements in this study are performed by using a computer interfaced LCR HITESTER. Two sets of electrical measurements are carried out. One is from room temperature ~27 to 200 °C at various frequencies with a heating rate of 2 °C/min and another is from 180 Hz to 1 MHz frequency at various temperatures for the evaluation of electrical properties of both RSFREC and DSFREC.

The dielectric constant (ε_r) is calculated from the capacitance using the equation:

$$\varepsilon_r = Ct/\varepsilon_0 A$$

where ε_r is the relative dielectric constant of the material, ε_0 is the permittivity of air, C is the capacitance, A is the area of cross section, and t is the thickness of the sample.

Results and discussion

The XRD patterns of both dewaxed and raw sisal fibers are shown in Fig. 1. The full width at half maximum (FWHM) of the diffraction peaks of both raw and dewaxed samples are analyzed. The $K_{\alpha 2}$ components of the peaks are stripped from the data by Philips Xpert Highscore software. The diffractograms of both dewaxed and raw sisal fiber display a well-defined main peak around $2\theta = 22.5°$, which is the characteristic of cellulose I [16]. Table 1 shows the crystallite size and degree of crystallinity of dewaxed and raw sisal fibers. It can be seen, after dewaxing the degree of crystallinity of the fiber has been increased, which may be due to the reduction of lignin content of the sisal fiber and the rearrangement of the cellulose chain. The changes in the crystalline peaks in Fig. 1 of dewaxed sample denote the changes in the crystalline region. The increasing

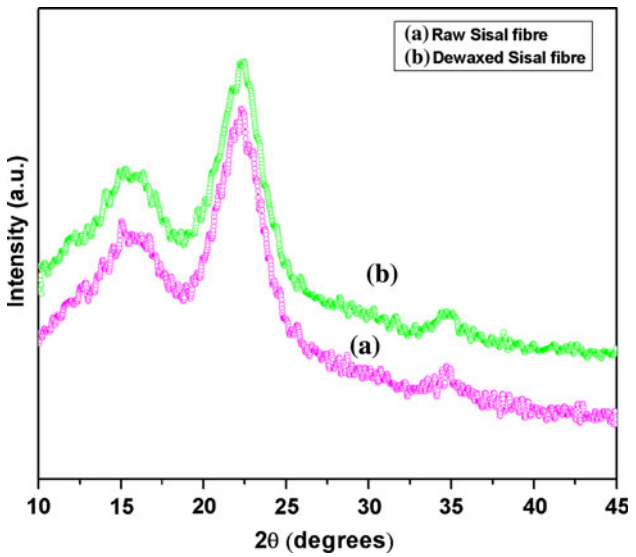

Fig. 1 WAXD patterns of raw sisal fiber and dewaxed sisal fiber

Table 1 The crystallite size and degree of crystallinity of raw and dewaxed sisal fibers

Sisal fiber	Crystallite size (Å)			Degree of crystallinity (%)
	Peak I ($2\theta = 15.5°$)	Peak II ($2\theta = 22.5°$)	Peak III ($2\theta = 34.8°$)	
Raw	38.02	30.48	35.5	62
Dewaxed	28.15	30. 87	49.15	67

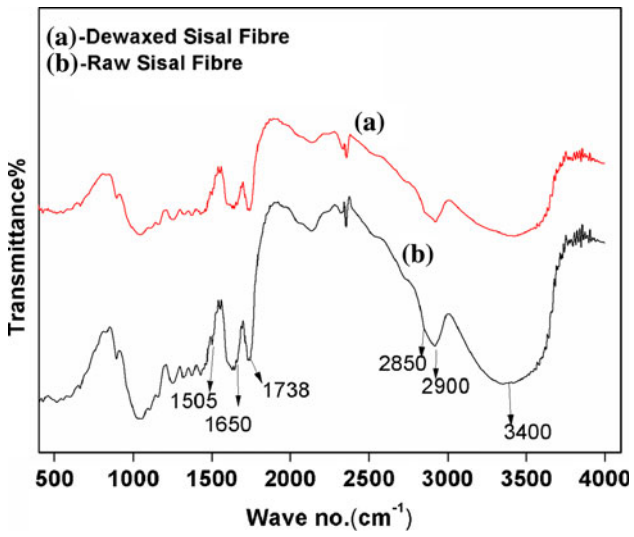

Fig. 2 IR spectra of raw sisal fiber and dewaxed sisal fiber

Table 2 The absorbance intensity ratio of individual band of IR spectra

Position of bands (cm^{-1})	Assignment	Raw	Dewaxed
3400	H–O stretching (H bonded)	1.12385	1.03279
2900	C–H stretching in methyl and methylene	1	1
2850	Wax peak	1.0591	0.98128
1735	C–O stretching in carbonyl and unsaturated β-ketone	1.04096	0.9779
1600–1650	Absorbed water in cellulose	1.07451	0.97937
1505	Aromatic ring of lignin	0.97451	0.94331

percent of crystalline peak area relative to the whole diffraction area suggests an improvement in the degree of crystallinity of the dewaxed fiber. The increase in the dimension and size of the crystallites may be due to the decrease in crystal distortion and defects [17].

Figure 2 shows the FTIR spectra of dewaxed and raw sisal fiber. The 2900 cm^{-1} band has been selected as internal band for the comparative studies of the spectra as it is present prominently in all the spectra of fiber sample. The absorbed intensity ratio is denoted as (A_b/A_{2900}) for maximum absorbance of the individual bands and are given in detail in the Table 2. The broad intense peak at $\sim$3400 cm^{-1} in raw sisal fiber is due to the O–H stretching for hydrogen-bonded hydroxyl group present in polysaccharide. However, this peak gets narrower and less intense in the case of dewaxed fiber because of the reduction of the O–H group which is further confirmed by the decrease in absorbance intensity ratio. The weak peak which is at $\sim$1738 cm^{-1} in raw sisal fiber is due to the presence of hemicelluloses and can be assigned to the C=O stretching.

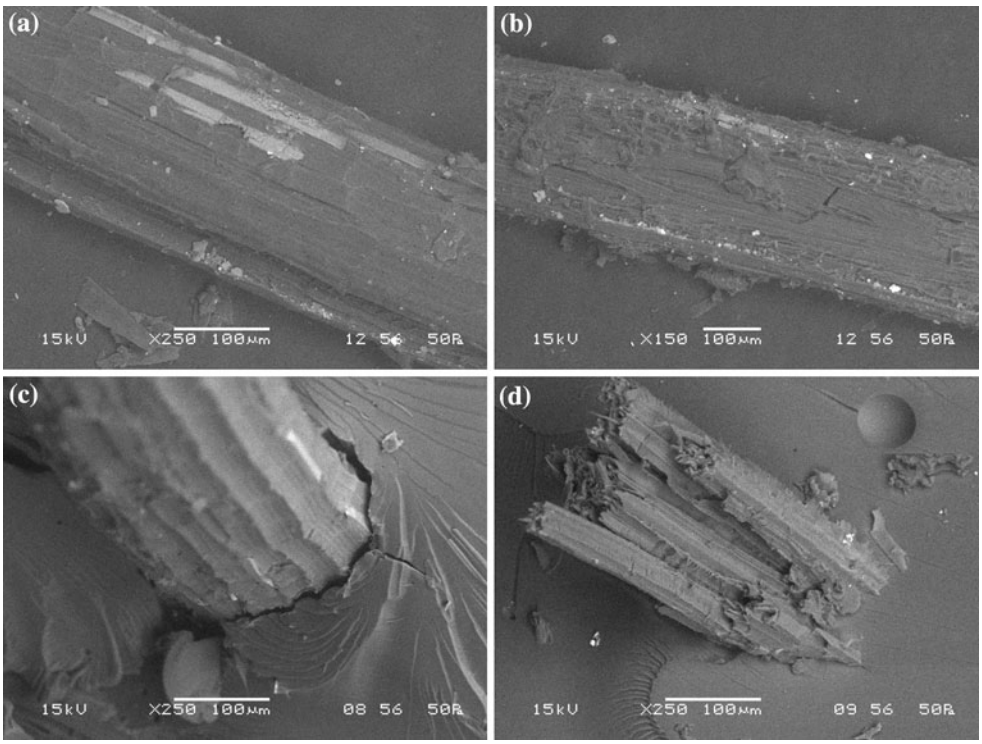

Fig. 3 **a**, **b** Longitudinal section of raw sisal fiber and dewaxed sisal fiber, respectively. **c**, **d** Fractured surface of RSFREC and DSFREC, respectively

It is found that the absorbance intensity ratio of this peak decreases after dewaxing, which suggests that dewaxing is responsible for the partial removal of hemicelluloses in the fiber. Similar is the case for the wax peak observed $\sim$2850 cm^{-1} in dewaxed fiber which is reduced in comparison to the raw fiber. This indicates that weaving size potato wax has been removed partially from the sisal fiber. It appears that during dewaxing substantial portion of uronic acid, a constituent of hemicelluloses and xylene has been removed, resulting in reduction of this peak. The weak broad peak that occurs in raw sisal fiber $\sim$1600–1650 cm^{-1} is associated with water absorbed in cellulose [18]. Here also the absorbance intensity ratio decreases due to dewaxing. The aromatic ring of lignin band ($\sim$1505 cm^{-1}) shows a decreased absorbed intensity ratio after dewaxing which confirms the reduction of lignin content in the dewaxed fiber [19].

The density of the raw fiber is found to be $\sim$1.32 g/cc whereas for the dewaxed fiber it came out to be $\sim$1.39 g/cc. The increase in density of the dewaxed fiber may be due to the partial removal of the wax and impurities. The rearrangement of the fibrils in a more compact manner may also be leading to the closer packing of the cellulose chain structure after dewaxing.

The longitudinal morphologies of raw and dewaxed sisal fibers are shown in the Fig. 3a, b, respectively. It is observed that the surface roughness of the fiber has been increased significantly after dewaxing. Again, because of the removal of the surface impurities and cementing material like lignin and hemicelluloses, separation of the ultimate cells has increased. This leads to the increase in effective surface area of the fiber to become more compatible with the matrix. The partial removal of waxy material in dewaxed fiber has also increased the interfabrillar region and gives a rough morphology. Figure 3c, d shows the fractured surfaces of both RSFREC and DSFREC, respectively. The mechanism of failure in case of RSFREC is clear from the fractured surface of the composite. The adhesion between fiber and matrix is poor, which is shown by gap around the fiber at the interface whereas in DSFREC the fiber matrix adhesion is shown by fiber breakage rather than fiber pullout.

The Fig. 4 shows the flexural strength and tensile strength of both RSFERC and DSFREC. In both the cases the strength of DSREC is found to be higher than the RSFERC. It is well known that for fiber-reinforced composites, the interfacial zone plays a leading role in transferring the load between fiber and matrix which consequently affects the mechanical properties such as strength [20–22]. This finding demonstrates that flexural failure depends mainly on the fiber/matrix adhesion. The increased value of flexural strength and tensile strength in case of DSFREC may be due to the increase in effective surface area available for contact with the matrix [23].

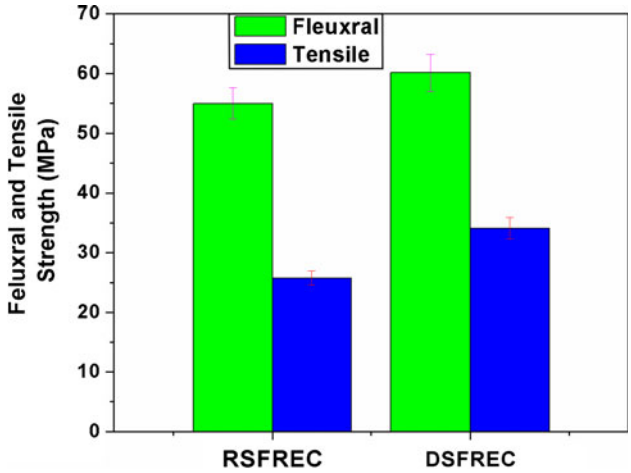

Fig. 4 Flexural strength and tensile strength of RSFREC and DSFREC

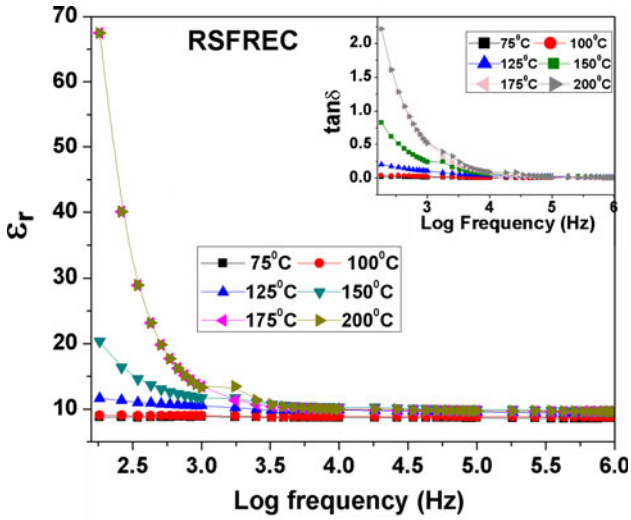

Fig. 5 Variation of ε_r with frequency in RSFREC. *Inset* Variation of tanδ with frequency in RSFREC

The removed cementing material of the dewaxed fiber is replaced by epoxy during composite formation which creates a reactive bond between them with increased static force because of the rough surface of the fiber. Hence, from the mechanical point of view, the dewaxing of fibers is beneficial since it reinforces the fibers/matrix load transfer.

Figures 5 and 6 show the frequency dependence of ε_r of both RSFREC and DSFREC, respectively, in a temperature range from 75 to 200 °C, whereas the plot in the inset of the above figures shows the frequency dependence of tanδ in the same specified range of temperature. It is found that in both cases with increase in frequency the value of ε_r as well as tanδ decreases. The change of ε_r and tanδ at lower frequency region is higher than at very high frequency. Generally, the dielectric constant (ε_r) of a polymeric

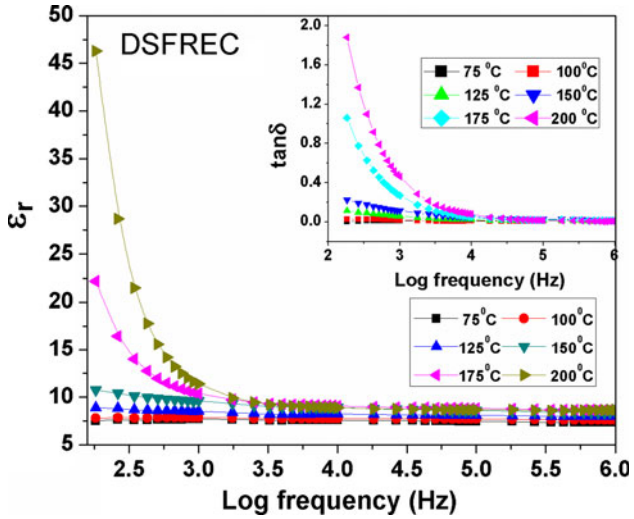

Fig. 6 Variation of ε_r with frequency in DSFREC. *Inset* Variation of tanδ with frequency in DSFREC

material depends mainly on interfacial and dipole polarization. The interfacial polarization is prominent in heterogeneous material and is highest at lower frequency. Hence, the higher values of ε_r and tanδ at low frequency can be explained in terms of interfacial polarization and the free motion of dipoles within the material which is connected to ac conductivity relaxation. It is found that the value of ε_r for the DSFREC has been decreased in comparison to the RSFREC. The overall dielectric properties in a polymeric composite are the contribution of both the crystalline and amorphous regions. Usually, the amorphous regions make the major contribution to both ε_r and tanδ. As a result, ε_r and tanδ decreases with an increasing degree of crystallinity [24].

Figures 7 and 8 show the temperature dependence of ε_r of both RSFREC and DSFREC at four different frequencies whereas the plot in the inset of the above figures shows the temperature dependence of tanδ at specified frequencies. The room temperature (RT) ε_r values of RSFREC and DSFREC at 1 kHz frequency are found to be $\sim$7.81 and 7.29, whereas the tanδ values are $\sim$0.015 and 0.013, respectively. It is observed that with the rise in temperature, ε_r and tanδ value for both RSFREC and DSFREC increases. An exothermic peak is observed in the plot of ε_r versus temperature $\sim$130 °C at 1 kHz frequency in both samples which confirms the presence of a relaxation process. This relaxation is named as α relaxation (glass–rubbery transition). Further with increase in frequency this relaxation shifted toward higher temperature side. The relatively high values of ε_r and tanδ at high temperature is attributed to the enhanced mobility of large parts of the polymer chains and the co-operating contribution of interface polarization [weak Maxwell–Wagner–Sillars (MWS)]

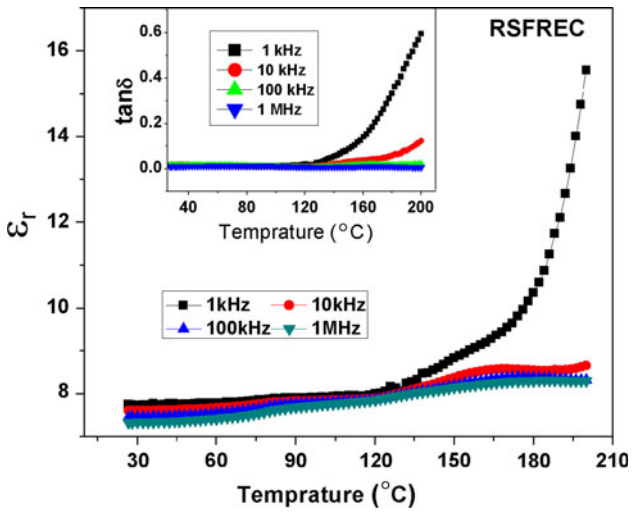

Fig. 7 Variation of ε_r as a function of temperature for the RSFREC. *Inset* Variation of tanδ as a function of temperature for the RSFREC

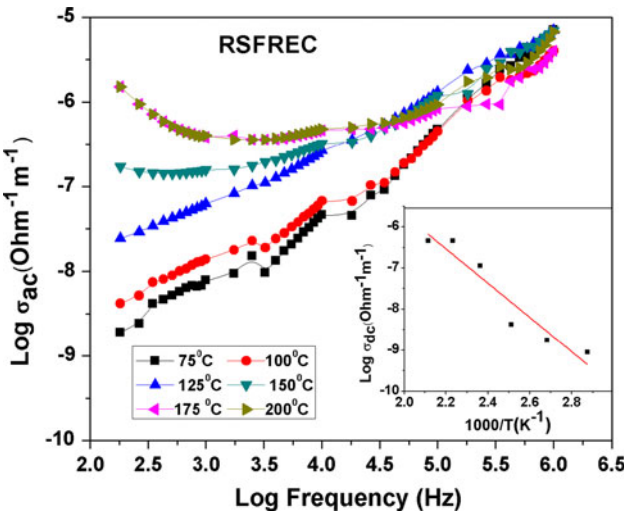

Fig. 9 Frequency dependent ac conductivity for the RSFREC. *Inset* Variation of dc conductivity against 10^3/T RSFREC

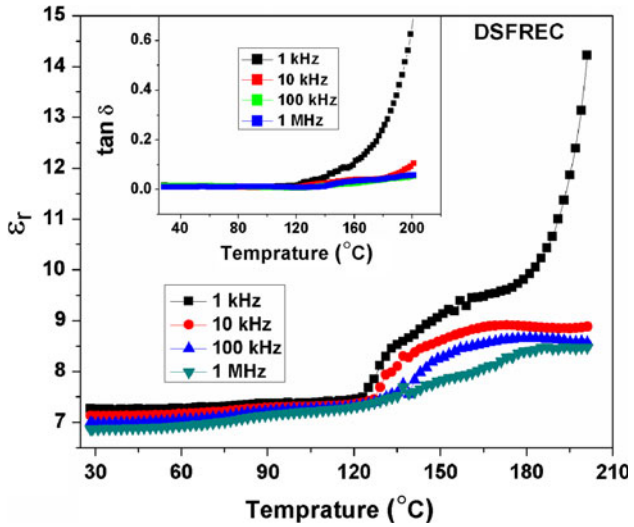

Fig. 8 Variation of ε_r as a function of temperature for the DSFREC. *Inset* Variation of tanδ as a function of temperature for the DSFREC

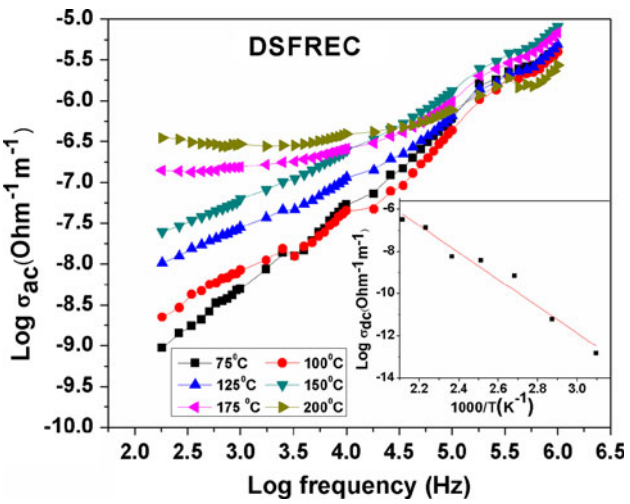

Fig. 10 Frequency dependent ac conductivity for the DSFREC. *Inset* Variation of dc conductivity against 10^3/T DSFREC

effect in the composite systems which arise due to additives, plasticizers etc. in polymer composite.

The frequency dependence of ac conductivity (logσ_{ac}) of DSFREC and RSREC at different temperatures in a wide range of frequencies in logarithmic scale are shown in Figs. 9 and 10, respectively. The σ_{ac} was calculated using an empirical relation i.e.,

$$\sigma_{ac} = \omega\varepsilon_r\varepsilon_0\tan\delta$$

where ε_0 is the permittivity of free space, and ω is the angular frequency. The σ_{ac} patterns show a frequency independent behavior in the low frequency region and exhibits dispersion at higher frequencies. This behavior satisfies the universal power law:

$$\sigma(\omega) = \sigma_0 + A\omega^n$$

where σ_0 is the dc conductivity, A is the pre-exponential factor, and n is the fractional exponent, whose value lies in between 0 and 1. It is observed that σ_{ac} for DSFREC and RSREC increases with the increase in temperature and that confirms the negative temperature coefficient of resistance behavior. This behavior also suggests that the electrical conduction in the sample is increasing at the higher temperature which may be due to the increase in the segmental mobility of the polymer molecules. It can also be seen that ac conductivity decreases with decrease in frequency and becomes independent of frequency after a certain limit. Dc conductivity (σ_{dc}) has been calculated by

extrapolating this toward the lower frequency side, which follows Arrhenius law given by:

$$\sigma_{dc} = \sigma_0 \exp[-E_a/K_\beta T]$$

where E_a is the activation energy of conduction and T is the absolute temperature. The plot in the inset of Figs. 9 and 10 shows the variation of dc conductivity ($\log\sigma_{dc}$) against 10^3/T. The nature of variation is almost linear over a wide temperature range. The slope of the linear least squares fitting of the data gives the values of activation energy (E_a) ~0.82 and 1.41 eV, respectively, for RSFREC and DSFREC. The lower value of activation energy is obtained in case of RSFREC may be due to the decrease in the height of the potential barrier between two orientational conformation states and in resulting from molecular motion. As the potential barrier between two orientational conformation states in case of RSFREC is lower than the DSFREC, the movement of the molecules becomes relatively easier, which in turn increases the ε_r, tanδ, and σ_{dc} in the sample.

Impedance spectroscopy has been considered as a powerful technique for characterization of dielectric materials. The use of modulus spectroscopy plot is particularly useful for separating the components with similar resistance but different capacitance. In this study, we have adopted the formalism of electric modulus to minimize the effect of σ_{dc} and to suppress the electrode effect [25, 26]. The complex electric modulus (M^*) has been calculated from the impedance data using the following relation:

$$M^* = M' + jM'' = 1/\varepsilon^* = j\omega C_0 Z^*$$

where $M' = \omega C_0 Z''$, $M'' = \omega C_0 Z'$, $j = \sqrt{(-1)}$, ω (angular frequency) $= 2\pi f$, C_0 = geometrical capacitance of the sample $= \varepsilon_0 (A/t)$, ε_0 = permittivity of free space, A = area of the electrode surface, and t thickness of the sample.

Figures 11 and 12, respectively, show the variation of real parts of the complex modulus (M') of RSFREC and DSFREC with frequency over a wide range of temperature. It is found that the values of M' increase with frequency at each temperature and have finally reached a constant value, on the other hand, the frequency variation of ε_r has been decreased almost to a constant value. This behavior is exactly opposite to the variation of ε_r with frequency. The evolution of M' toward a constant value at the high frequency region is due to the fact that polarization becomes ineffective to the applied field at higher frequency. The existence of a step-like transition from low to high values of M' is evident in all specimens, at temperatures higher than 100 °C. The recorded transitions imply the presence of a relaxation process, which should be accompanied by a loss peak in the diagrams of the imaginary part of electric modulus (M'') versus frequency. Again, it is also observed that the M' value in case of DSFREC is higher than the

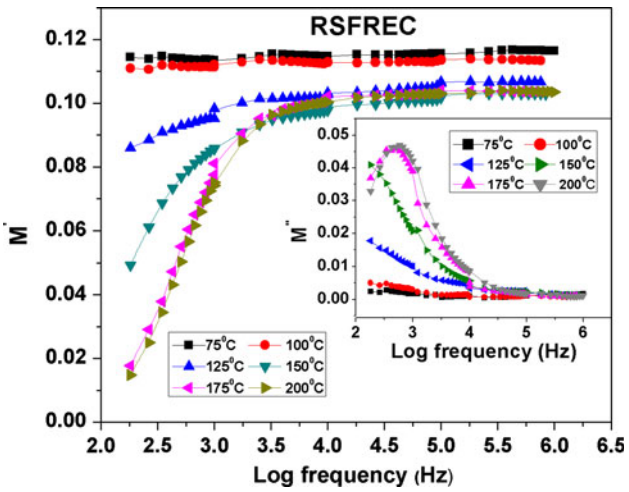

Fig. 11 Variation of M' as a function frequency for the RSFREC. *Inset* Variation of M'' as a function frequency for the RSFREC

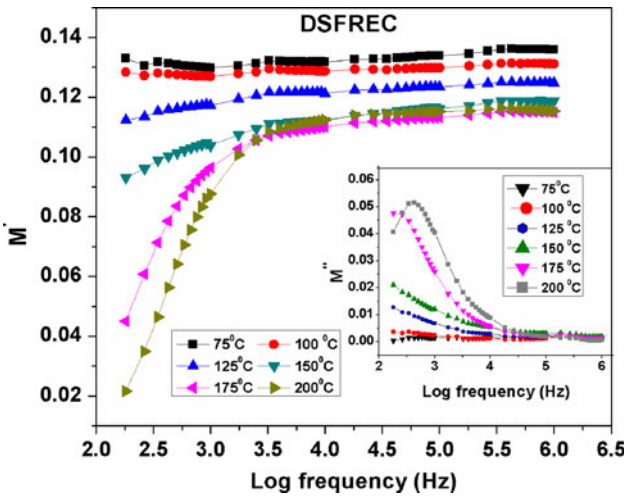

Fig. 12 Variation of M' as a function frequency for the DSFREC. *Inset* Variation of M'' as a function frequency for the DSFREC

RSFREC, which is in good agreement with the dielectric data.

The variation of the imaginary part of the electric modulus (M'') of both RSFREC and DSFREC with frequency at selected temperature is shown in the inset of the Figs. 11 and 12, respectively. The shifting of relaxation peaks with rise in temperature ascribing correlation between motions of mobile ions, which suggests that there is a spread of relaxation times. The relaxation mechanism at lower temperature and lower frequency is different from at higher temperature and higher frequency. The nature of the inset of the Figs. 11 and 12 suggests that there are other relaxations also present at a frequency lower than 100 Hz. It can be explained that the appearance of loss peak ~130 °C is may be due to the presence of glass/rubber transition and after 130 °C, it may be attributed to the

presence of interfacial polarization. Hence, it is clear that the behavior of M'' is nearly same in case of both RSFREC and DSFREC i.e., different kinds of relaxation phenomena are present in both cases.

Conclusions

Sisal fiber has been modified by dewaxing which results an increment in the degree of crystallinity, crystallite size, and the density of the dewaxed fiber. This fact may be due to rearrangement of cellulose chains and removal of internal constraints. Better flexural strength and tensile strength has been reported in case of DSFREC because of the removal of cementing materials and that may be obviously due to the increased adhesion between fiber and matrix. The observed decrease in the value of ε_r in case of DSFREC may be attributed to the reduction in O–H group and absorbed water which in turn decreases the orientation polarization. Better interlocking between the fibers and matrix have hindered the free molecular motion of the molecular chain in the composite interface in DSFREC, which may also lead to the decrease in value of ε_r, $\tan\delta$, and σ_{dc}, but an increment in the flexural strength and tensile strength. The SEM micrograph of fractured surface of DSFREC confirms the better wetting of the fiber by the matrix which in turn increases both flexural strength and tensile strength of the composite. The σ_{dc} is found to follow the Arrhenius relation for both DSFREC and RSFREC. The activation energy DSFREC is found to be higher than that of RSFREC indicating a rigidification of the fibre–matrix interfacial region. Modulus spectra confirm the presence of different relaxation mechanism in the composite.

This study enables us to confirm that there exists a good correlation between dielectric behavior and mechanical properties of epoxy reinforced by sisal fiber. Beside that both electrical and mechanical properties of the composites have also been correlated with the structural parameters of the reinforced fiber.

Acknowledgements Profound appreciation and gratitude is extended to one and all the members of the Department of Physics, and the Director NIT Rourkela for their cooperation during completion of the manuscript of this article. We must thank Dr. Sitangshu Sarkar, Scientist-in-Charge, Sisal Research Station (ICAR), Bamra, Orissa (INDIA) for his kind cooperation for providing us the sisal fibre for this study.

References

1. Shah AN, Lakkad SC (1981) Fibre Sci Technol 15:41
2. Bisanda ETN, Ansell MP (1991) J Compos Sci Technol 4:165
3. Kulkarni AG, Satyanarayana KG, Rohtagi PK (1981) J Mater Sci Lett 16:1720
4. Dutta AK, Mukherjee PS, Mitra CB (1980) J Mater Sci 15:1856. doi:10.1007/BF00550607
5. Patra A, Bisoyi DK (2010) J Mater Sci 45:5742. doi:10.1007/s10853-010-4644-8
6. Rong MZ, Zhang MQ, Liu Y, Yang GC, Zeng HM (2001) Compos Sci Technol 61:1437
7. Feng DAAN, Caulfield DF, Sanadi AR (2001) Polym Compos 22:506
8. Nosbi N, Akil HM, Ishak ZAM, Bakar AA (2011) Bioresources 6:950
9. Marcia CB, Alessandra LM, Marcio K, Jose DA, Antonio DN (2009) Amaz Phoenix Proj Sustain 1:1431
10. Khan NMD (1991) Ph. D Thesis. pp 71–72
11. Roy SC (1960) Text Res J 30:451
12. Ratho T, Torasia S, Mohanty JC (1964) Indian J Phys 38:28
13. Klata E, Krucinska I, Borysiak S, Garbarczyk J, Katedra M, Wlokienniczej P, Lodzka L (2003) Pol Kompoz 3:332
14. Borysiak S, Doczekalska B (2005) Fibres Text East Eur 13:87
15. Rosa IMD, Santulli C, Sarasini F (2010) Mater Des 31:2397
16. Klemm D, Heublein B, Fink H, Bohn A (2005) Angew Chem Int Ed 44:3358
17. Liansong W, Dongling H, Tianyao Z, Lifang Z, Chengdong X (2010) Cryst Res Technol 45:275
18. Troedec ML, Peyratout C, Chotard T, Bonnet JP, Smith A, Guinebretiére R (2007) In: 10th International Conference of the European Ceramic Society, Berlin, pp 451–456
19. Mahato DN, Prasad RN, Mathur BN (2009) Indian J Pure Appl Phys 47:643
20. Trindade WG, Hoareau W, Megiatto JD, Razera IAT, Castellan A, Frollini E (2005) Biomacromolecules 6:2485
21. Georgopoulos ST, Tarantili PA, Avgerinos E, Andreopoulos AG, Koukios EG (2005) Polym Degrad Stab 90:303
22. Thielemans W, Wool RP (2005) Biomacromolecules 6:1895
23. Bisanda ETN (1991) Ph. D Thesis
24. Hanna AA, Atef AI, Salwa O, Heikal SO (2003) J Polym Sci Polym Chem Ed 18:1425
25. Turnhout JV, Wübbenhorst M (2002) J Non-Cryst Solids 305:50
26. Hammami H, Arous M, Lagache M, Kallel A (2006) Compos Part A1 37:8